RSC Advances

ROYAL SOCIETY OF CHEMISTRY

www.rsc.org/advances

Effect of hydrophobic montmorillonite on PVDF and PEI hollow fiber membranes in gas-liquid contacting process: a comparative study

M. Rezaei-DashtArzhandi[a], A. F. Ismail [a,*], Gh. Bakeri [b], S.A. Hashemifard [c], T. Matsuura [a,d]

[a] Advanced Membrane Technology Research Centre (AMTEC), Universiti Teknologi Malaysia, 81310 Skudai, Johor, Malaysia

[b] Advanced Membrane and Biotechnology Research Centre, Faculty of Chemical Engineering, Babol Noshirvani University of Technology, Babol, Iran

[c] Chemical Engineering Department, Engineering Faculty, Persian Gulf University. Bushehr, Iran

[d] Industrial Membrane Research Institute, Department of Chemical and Biological Engineering, University of Ottawa, 161 Louis Pasteur St., Ottawa, ON, K1N 6N5, Canada

[*]Corresponding author email: afauzi@utm.my

Tel.: +60 7 5535592; fax: +60 7 5581463

Abstract

Porous polyvinylidenefluoride (PVDF) and polyetherimide (PEI) hollow fiber mixed matrix membranes (MMMs) were spun under the same spinning conditions for CO_2 absorption experiment via membrane contactor. The effects of montmorillonite (MMT) loading on thermodynamic and kinetic aspects of phase inversion as well as the membrane properties were investigated using various analytical characterization methods. MMT embedment into PVDF lowered thermodynamic stability while making the solvent/nonsolven exchange in the phase inversion faster, which resulted in the formation of thinner skin layer, thicker finger-like layer and thinner sponge-like layer. As a result, the N_2 gas permeance increased considerably. As for the PEI, the high hydrophobicity of the incorporated clay particles slowed down the rate of solvent/nosolvent exchange and subsequently thicker skin layer as well as more compact

sublayer structure with narrower finger-like pores was formed. Hence, a considerable reduction in the rate of gas permeation for the PEI MMMs was observed. In addition, both PVDF and PEI membranes experienced significant increase in the contact angle and LEPw by the presence of hydrophobic MMT in the system. Physical CO_2 absorption with distilled water was performed using the hollow fiber gas–liquid membrane contactor. The absorption flux was enhanced by the MMT embedment for both PVDF and PEI but the flux enhancement of PEI was more pronounced than the PVDF However, the long-term absorption stability test over 15 days revealed that the flux of the MMT incorporated PEI hollow fiber deteriorates considerably with time due to the intrinsically high hydrophilicity of PEI material.

Keywords: Carbon dioxide removal, Polyvinylidenefluoride; Polyetherimide; Hydrophobic montmorillonite; Hollow fiber mixed matrix membrane; Phase inversion; Membrane contactor.

1.0 Introduction

Porous hydrophobic membranes have rapidly developed in recent years to remove CO_2, one of the major greenhouse gases, through gas-liquid membrane contactors [1]. Membrane contactors are devices providing a direct contact of gaseous and liquid phases for the purpose of mass transfer between the phases without dispersing one phase into the other. Since the diffusivity in gas phase is 10^4 times higher than the liquid phase, the penetration of liquid into membrane pores drastically reduces the contactor performance. Hence, the wettability of membrane pores during operation should be considered as one important parameter in membrane contactor applications. In order to prevent the liquid from entering into the membrane pores, a trans-membrane pressure

less than the membrane liquid entry pressure of water (LEPw) must be applied. The pressure can be calculated via the Laplace-Yang equation:

$$LEPw = \frac{4\delta_L Cos\theta}{d_{\max}} \quad \textbf{(1)}$$

where δ_L is the surface tension of liquid absorbent and; θ is the contact angle between the liquid absorbent and prepared membranes, $d_{\max}$ is the maximum pore diameter.

The approaches of increasing LEPw include increasing membrane-water contact angle and reducing the surface pore size. However, the size of the membrane pores should be astutely optimized since reducing pore size, along with decreasing surface porosity and increasing tortuosity, lowers the permeation flux while large pore size increases the possibility of pore wetting. In addition, the membrane should have sufficient chemical, thermal and mechanical stabilities [2].

Therefore, conventional polymeric materials of high surface contact angle such as polytetrafluoroethylene (PTFE), polypropylene (PP), polyethylene (PE), and polyvinyllidenefluoride (PVDF) are favourable materials to fabricate high hydrophobicity membranes. Unlike PTFE, PP and PE, PVDF is easily dissolved in organic solvents facilitating fabrication of membranes via phase inversion method which is the most flexible fabrication technique with excellent control on the pore size, pore size distribution and porosity [3-7]. However, PVDF has a small critical surface tension (25 dyn/cm), which restricts the penetration of non-solvent, usually water, into the nascent membranes during phase inversion process. Consequently, slow solidification during phase inversion causes as-spun PVDF fibers to possess

low porosity, resulting in low mass transfer rate [8]. On the other hand, conventional thermoplastics like PEI with lower viscosity than PVDF when dissolved into solvent can be more convenient to fabricate highly porous membranes. PEI is a polymer with T_g higher than the operation gas-liquid contacting processes temperatures allowing PEI membranes to withstand harsh contactor operating conditions. However, water contact angle of PEI less than 90° allows absorbent droplets to easily drive to the capillary.

Tremendous researches on improving surface porosity and structure of PVDF as well as the hydrophobicity of PEI membranes to intensify their contactor process performances during long-term operations have been conducted [6, 9]. It should be mentioned that a stable long-term membrane performance depends on the membrane hydrophobicity and structure [10].

One of the approaches was to modify the membrane structurally by introducing some kinds of additives into the solutions. Mansourizadeh and Ismail [11] structurally modified asymmetric PVDF hollow fiber membranes for CO_2 absorption through contactor system by introducing lithium chloride (LiCl) as a pore former additive into the spinning solution. The permeation rate and performance of the modified membranes were improved without increase of the surface hydrophobicity. Recently, the surface modifying macromolecules (SMMs) were used by Mansourizadeh [12] and Bakeri [13] to increase the hydrophobicity of PVDF and PEI membranes. The surface modified membranes exhibited significantly higher permeance and CO_2 absorption flux than the original membranes and several commercial PVDF, PTFE and PP membranes. However, using SMMs for membrane surface modification came together with some unwanted

structural changes such as increasing pore size and reducing porosity, which can render the long-term stability undesirable.

Fabrication of polymer-inorganic membranes, known as mixed matrix membranes (MMMs), is an alternative method to modify membrane properties and performance. Incorporation of inorganic particles into polymer matrix in addition offers improvements in physical, thermal and chemical stability of membranes in aggressive environments. In fact, the structure of the final membranes is a function of physical and chemical properties of both polymer and inorganic particles. Several studies proved that skin layer surface porosity, thickness and contact angle can be influenced by nanoparticle embedment. The permeation rate is hence affected by the presence of nanopartilces since the permeation rate is influenced by the skin layer properties as well as the structure of the sublayer of the membranes. Both of these structurally distinct membrane regions (skin and support) govern the permeation rate; the skin layer is responsible for the permeability of the membrane, while the sublayer affects the contactor performance by its compaction behavior.

It was reported that the addition of very small amounts of layered silicates significantly improves the thermal and mechanical properties of the membrane [14]. The surface contact angle of the membrane also was found to reduce if the added clay particles were hydrophilic [15]. Moreover, membrane pore size, surface porosity and permeability also could be enhanced by the addition of clay particles in the casting dope. However, contrary results on the effect of layered silicate materials on the permeability of prepared MMMs can be found in the literature. Yano [16] reported a remarkable decrease of the permeation flux when the MMT clay particles were incorporated

into polyamide polymer matrix. The flux increase or decrease therefore seems to depend on the type of the fillers used as well as their dispersion to the polymer solutions. It can be said that the success of fabricated MMMs is highly dependent on the choice of the polymer matrix and the inorganic filler as well as the control of the interfacial properties between the polymer and the filler.

Our previous publications have revealed that the PVDF and PEI membranes with incorporated hydrophobic MMT can be effectively utilized in gas-liquid contacting processes. However, the performance of hydrophobic MMT/polymer MMMs may depend on the hydrophobicity/philicity of the host polymers but their effects are still not completely understood.

Hence, the objective of this work is to compare the effects of embedding hydrophobic MMT nanoparticles on the properties of host PVDF and PEI matrixes which are, respectively, hydrophobic and hydrophilic. To the authors' best knowledge, no study has been done to compare PVDF and PEI membranes when they are fabricated with the incorporation of the same inorganic nanoparticles in CO_2 absorption via contactor system. In particular, the comparison is made for the effects of the hydrophobic MMT on the thermodynamic and kinetics that are involved in the phase inversion process. To this end, the pore size, porosity, contact angle, wetting resistance, mechanical stability and the performance in CO_2 absorption by gas-liquid membrane contacting process of the fabricated membranes are thoroughly investigated.

2. Experimental

2.1. Materials

Polyvinylidenefluoride pellets (Kynar® 740, Arkema Inc., PA, USA) and polyetherimide (PEI, Ultem®, General Electric Company) were used as the base polymer. 1-Methyl-2-pyrrolidone (N-Methyl-2-pyrrolidone, NMP, 99.5%) was used as the solvent. MHydrophobic montmorillonite (MMT) modified by octadecylamine (25–30 wt.%) with a surface hydrophobicity of almost 95 º was purchased from Fluka. Lithium chloride (LiCl) and ethanol with purity more than 96% were purchased from Sigma–Aldrich® and MERCK respectively and used as non-solvent additives to induce a fast phase-inversion process [17, 18]. Tap water and distilled water were used as coagulant and liquid absorbent, respectively. Methanol (GR grade, 99.9%) was supplied from MERCK and used for post-treating the fabricated membranes.

2.2. Fabrication of hollow fiber MMMs

Hollow fiber MMMs were spun via the phase inversion method. The details of the experimental set up and the experimental procedure were described elsewhere [19]. The solutions containing the different polymer types, pore formers and MMT dosages were prepared. MMT in the amount of 1.0, 3.0 and 5.0 wt.% of polymers was dispersed in the solvent (NMP) and sonicated for 1 h at 40 ^{o}C to disintegrate MMT agglomerates. LiCl and ethanol as pore formers for the PVDF and PEI, respectively were added to the mixture. The polymers were then gradually added and the mixture was stirred overnight to ensure the complete dissolution of the polymer. It should be mentioned that the composition of the PVDF and PEI spinning solutions were brought from the literature in their optimum range [11, 20, 21]. The prepared spinning dopes were degassed by ultra-sonication and maintained for 5 h at room temperature before the use for spinning. The viscosity of the prepared polymer dopes was measured by viscometer (EW-98965-40, Cole-parmer, USA).

The polymer dope was extruded from the spinneret (i.d. 0.55 mm, o.d. 1.2 mm) at the flow rate of 4.5 ml min^{-1} at 22 °C by applying nitrogen pressure and a syringe pump was used to deliver the bore fluid (water) to the center of the spinneret. Tap water at the temperature of 22 °C was used for the external coagulant. The spun fibers were kept immersed in water for 3 days at ambient temperature, with daily change of water to remove the residual solvent. Then, they immersed in methanol for 15 min for the post-treatment. The membranes were subsequently dried at ambient temperature before the characterization tests. The hollow fibers were coded hereafter depending on the polymer and the modified MMT loading as the detailed composition can be seen in Table 1.

Table 1: Composition of fabricated membranes

	Membrane							
Component	**M0**	**M1**	**M3**	**M5**	**P0**	**P1**	**P3**	**P5**
PVDF (%w/w)	18	18	18	18	-	-	-	-
PEI (%w/w)	-	-	-	-	15	15	15	15
LiCl (%w/w)	2.5	2.5	2.5	2.5	-	-	-	-
Ethanol (%w/w)	-	-	-	-	4	4	4	4
MMT (%w/w of polymer)	0	1	3	5	0	1	3	5
NMP (%w/w)	79.5	79.5	79.5	79.5	81	81	81	81

2.3. Scanning electron microscopy (SEM)

Scanning Electron Microscopy (SEM) (TM 3000, Hitachi) was used to examine the morphology of the fabricated PVDF and PEI hollow fiber MMMs, as well as the degree of adhesion between polymer matrix and fillers. The membrane samples were first immersed in liquid nitrogen and then fractured to obtain a smooth cross-section surface. The fractured fibers were placed on a disc and sputtered with a thin film of gold before testing. The SEM micrographs of the cross-section and the outside surface of the hollow fiber MMMs were taken at various magnifications.

2.4. Gas permeation and collapsing pressure tests

As the membrane in contactor application is porous, the pore size and porosity at the membrane surface play important roles in determining the performance. Hence, the gas permeation test was conducted to determine those surface parameters. The open end of the hollow fibers for the entry of gas/liquid flow was potted in a stainless steel housing, while the other end was sealed with epoxy glue. For gas permeation test, the nitrogen gas (N_2) was sent through the lumen side of the hollow fibers and the permeation rate of the gas coming out from the shell side was measured using a soap bubble flow meter. The conventional gas permeation testing model was used to obtain the structural parameters (Eqs. 2-3).

$$\bar{P} = P_P + P_K = \frac{2}{3}\left(\frac{8RT}{\pi M}\right)^{0.5}\frac{r_{P,m}}{RT}\frac{\zeta}{L_P} + \frac{1}{8\mu}\frac{r_{P,m}^2}{RT}\frac{\zeta}{L_P}\bar{p} \quad \textbf{(2)}$$

$$\bar{P} = A + B\bar{p} \quad \textbf{(3)}$$

where $\bar{P}$ is the total gas permeance ($mol\ m^{-2}\ Pa^{-1}\ s^{-1}$), P_P and P_K are gas permeance in Poiseuille and Knudsen flow regimes, respectively ($mol\ m^{-2}\ Pa^{-1}\ s^{-1}$), R is the universal gas constant ($8.314\ J\ mol^{-1}\ K^{-1}$), T is the absolute temperature (K), M is the molecular weight of gas ($kg\ mol^{-1}$), $r_{P,m}$ is the mean pore radius (m), μ is the viscosity of gas ($Pa\ s$), ζ is the surface porosity, L_P is the effective pore length (m) and $\bar{p}$ is the mean pressure (Pa) ($(p_u+p_d)/2$) where p_u is upstream pressure and p_d is downstream pressure. Using the intercept (A) and the slope (B) of $\bar{P}$ versus $\bar{p}$ plot, the mean pore size and the effective surface porosity can be calculated by Eqs. 4 and 5 [22-24].

$$r_{P,m} = \frac{16}{3}\frac{B}{A}\left(\frac{8RT}{\pi M}\right)^{0.5}\mu \quad (4)$$

$$\frac{\zeta}{L_P} = \frac{8\mu RTB}{r_{P,m}^2} \quad (5)$$

Improvement of the mechanical properties of polymeric membranes via nanoparticle incorporation is a design strategy that is earning considerable attention. Hence, collapsing pressure test to examine the mechanical stability of membrane was conducted. The test was performed during gas permeation test by increasing the upstream pressure at 0.5 bar interval until a sudden decrease or increase in the permeate flow in lumen side appeared.

2.5. Contact angle and liquid entry pressure of water (LEPw) measurement

Measuring the contact angle is a simple method of quantifying the hydrophobicity/philicity of the membranes. To measure the outer surface contact angle of the hollow fiber MMMs the sessile drop technique by a goniometer (model G1, Krüss GmbH, Hamburg, Germany) was used after the membranes were dried at 60 ± 2°C for 12 h. The measurement was made at various points to minimize the errors originating from the small diameter of the hollow fibers and then averaged.

Liquid entry pressure of water (LEPw) was measured to characterize the membranes in terms of wettability resistance. Distilled water was fed into the lumen side of the hollow fiber membranes using a diaphragm pump. The pressure was slowly increased at 0.5 bar interval and recorded as LEPw when the first water droplets appeared on the shell side surface of the hollow fiber MMMs.

2.6. Measurement of CO_2 absorption and long–term stability examination

The short-term CO_2 absorption experiment was carried out to evaluate the performance of the fabricated membranes where the distilled water and pure CO_2 were used as absorbent and solute gas, respectively. A total of 10 hollow fibers with the effective length of 17.5 cm were packed in a contactor module. Specifics of the membrane contactor modules were given in Table 2.

Table 2: Characteristics of membrane contactor module.

Module i.d. (mm)	14
Module length (mm)	250
Fiber o.d. (μm)	900-950
Fiber i.d. (μm)	530-590
Effective fiber length (mm)	175
Number of fibers	10

Distilled water flew on the lumen side in a countercurrent mode with pure CO_2 (P: 1 barg, flow rate: 1.2 L min^{-1}) on shell side during the absorption experiment. The liquid side pressure was kept 0.5 bar higher than gas side to prevent bubble formation on the liquid side. The CO_2 concentration in the liquid outlet at various flow rates was measured by chemical titration using 0.02 M sodium hydroxide (NaOH) solution and phenolphthalein to determine the CO_2 flux. The overall mass transfer coefficient (K_{OL}) can be calculated by Eq. 6.

$$K_{OL} = \frac{Q_L(C_L^{out} - C_L^{in})}{A\Delta C_L^{Av}} \quad \textbf{(6)}$$

where K_{OL} is overall mass transfer coefficient ($m\ s^{-1}$), Q_L is liquid flow rate ($m^3\ s^{-1}$), C_L is the solute gas (CO_2) concentration in liquid ($mol\ m^{-3}$), where the superscripts out and in are module outlet and module inlet, respectively. A is the contact area (m^2) which is calculated based on

inner diameter of the hollow fiber membrane as liquid flows in the lumen side and ΔC_L^{Av} is the logarithmic mean of transmembrane concentration difference of solute gas based on the liquid phase concentration ($mol\ m^{-3}$) which is calculated by Eq. 7.

$$\Delta C_L^{Av} = \frac{(HC_g^{in} - C_L^{in}) - (HC_g^{out} - C_L^{out})}{Ln((HC_g^{in} - C_L^{in})/(HC_g^{out} - C_L^{out}))} \quad \textbf{(7)}$$

where C_g is the CO_2 gas concentration ($mol\ m^{-3}$) and H is the Henry's constant.

The average flux can be calculated by a simple mass balance of CO_2 over the length of fiber as shown in Eq. 8:

$$J_{av} = \frac{Q_L HC_g(1 - \exp(-K_{OL}\pi d_i L / Q_L))}{\pi d_i L} \quad \textbf{(8)}$$

where J_{av} is absorption flux of CO_2, L is the length of hollow fiber (m), d_i is the inner diameter of hollow fiber (m).

In addition, the CO_2 absorption performance of the fabricated MMMs was examined over 350 h at the constant flow rates of the gas and liquid. In fact, the membrane absorption performance during a long period of time should be considered for further industrial implementation [25].

3. Results and discussion

3.1. Morphological studies

Formation of integrally skinned porous gas absorption membranes is primarily based on the wet phase inversion process. It involves the diffusive exchange of solvent and coagulant as liquid-liquid phase separation [26]. The solution progressively demixes until separates into two liquid phases, a polymer-rich phase and a polymer-lean phase. Subsequently, continuing the exchange

of solvent/coagulant, as long as the driving force for the spontaneous demixing exists, increases the polymer concentration in the polymer rich phase surrounding the polymer lean phase. Then, the polymer molecules rearrange their structure until a solidification of the concentrated phase occurs [4]. The polymer-rich phase forms the solid structure while the polymer-lean phase creates the membrane pores. In other words, the progressive exchange of solvent/coagulant leads polymer matrix to eventally precipitate, constituting the membrane. The final structure of the membrane is influenced by the rate of the precipitation throughout the phase inversion process; low precipitation rate creates symmetric structure, whereas high precipitation rate tends to make asymmetric membranes, differing in the sublayer and upper layer.

Therefore, it can be deduced that by controlling parameters of the phase inversion process, a variety of sublayer's morphologies such as finger-like or sponge-like as well as surface layers differing in the size of pores and pore number can be formed. Therefore, the stages strongly depend on thermodynamic stability of the solutions and the kinetic of solvent/coagulant exchange.

The phase inversion process commences with a thermodynamically stable solution and then the demixing of the components in the polymer solution occurs in the thermodynamically unstable condition to form two rich and lean polymer phases. The viscosity (kinetic aspect) of the solution as well interferes the rate of the phase separation.

The thermodynamic stability of polymer solution and the kinetics of phase inversion process depend on the spinning solution properties such as the type of polymer, viscosity and the presence of a nonsolvent or filler in the system.

As for the polymer type, the polymers with higher hydrophobicity and viscosity render higher thermodynamic stability than those of low contact angle [27]. PVDF as the first polymer of choice in this study is inherently a semi-crystalline polymer with high hydrophobicity and low surface tension (25 dyn cm^{-1}), which restricts the easy penetration of the coagulant into the nascent membrane during spinning process [8]. As a result, the PVDF membranes have randomly more packed structure with no discernible molecular order. On the other hand, PEI is an amorphous polymer with hydrophilic attributes and low solution viscosity; facilitating fast phase inversion, resulting in a more ordered molecular arrangement and an open structure compared to the PVDF in their solidified state.

Introducing hydrophobic MMT filler, whose surface was modified by hydrophobic tallow, into polymer solutions lowered the stability of solutions thermodynamically (thermodynamic effect), resulting in enhancement of liquid-liquid phase separation.

The membrane morphology is hence affected by the addition of hydrophobic MMT clay particles. No significant morphological differences are detected between the fabricated MMMs with different polymer type, hence the SEM images of M5 and P5 are used to represent all the MMMs in each clusters. In particular, lower thermodynamic stability of the PVDF/MMT solutions accelerates the early stage of the phase inversion process and greatly influences the

surface of the membrane; a thin skin layer with a large number of small pores is formed. The decrease of the skin layer thickness for clay/polysulfone composite membranes was observed by increasing clay loading [28]. In addition, the presence of the MMT clay in the PVDF solution slightly reduced the viscosity (see Table 3), similar to the observation made by Huang [29] where sepiolite (SP) nano-clay was added into the blend solution of chitosan and poly vinyl alcohol (PVA). However, the results are in contrast to the results reported by Zhang [30] and Li [31] where they added inorganic particles to the polymer solutions.

Decreasing solution viscosity by MMT addition was most likely attributed to the high percentages of surface modifiers (tallow) in the system which has sorrounded the MMT nano particles, dissolving in the solvent and thereby leads to decrease in the solution viscosity. Consequently, the mutual diffusion between coagulant (water) and solvent was accelerated (kinetic effect) and the coagulant inflow to the nascent membrane structure was facilitated. As a result, a large number of longer finger-like pores were formed underneath the thin skin layer, which met a thick sponge-like structure at the middle of the PVDF hollow fiber MMMs as was presented in the cross-sectional images (Fig. 1). In other words, as an effect of MMT clay incorporation into PVDF, the thickness of the finger-like area underneath the formed thin skin layer increased while the thickness of the sponge-like zone decreased. As was reported, the finger-like structure is formed at the rapid phase inversion while slow phase inversion tends to create sponge-like structure [21]. The observations indicate that in this particular system, both thermodynamic and kinetic effects of the added MMT clay particles played important roles to determine the PVDF MMMs' morphological changes of either top-layer or sublayer.

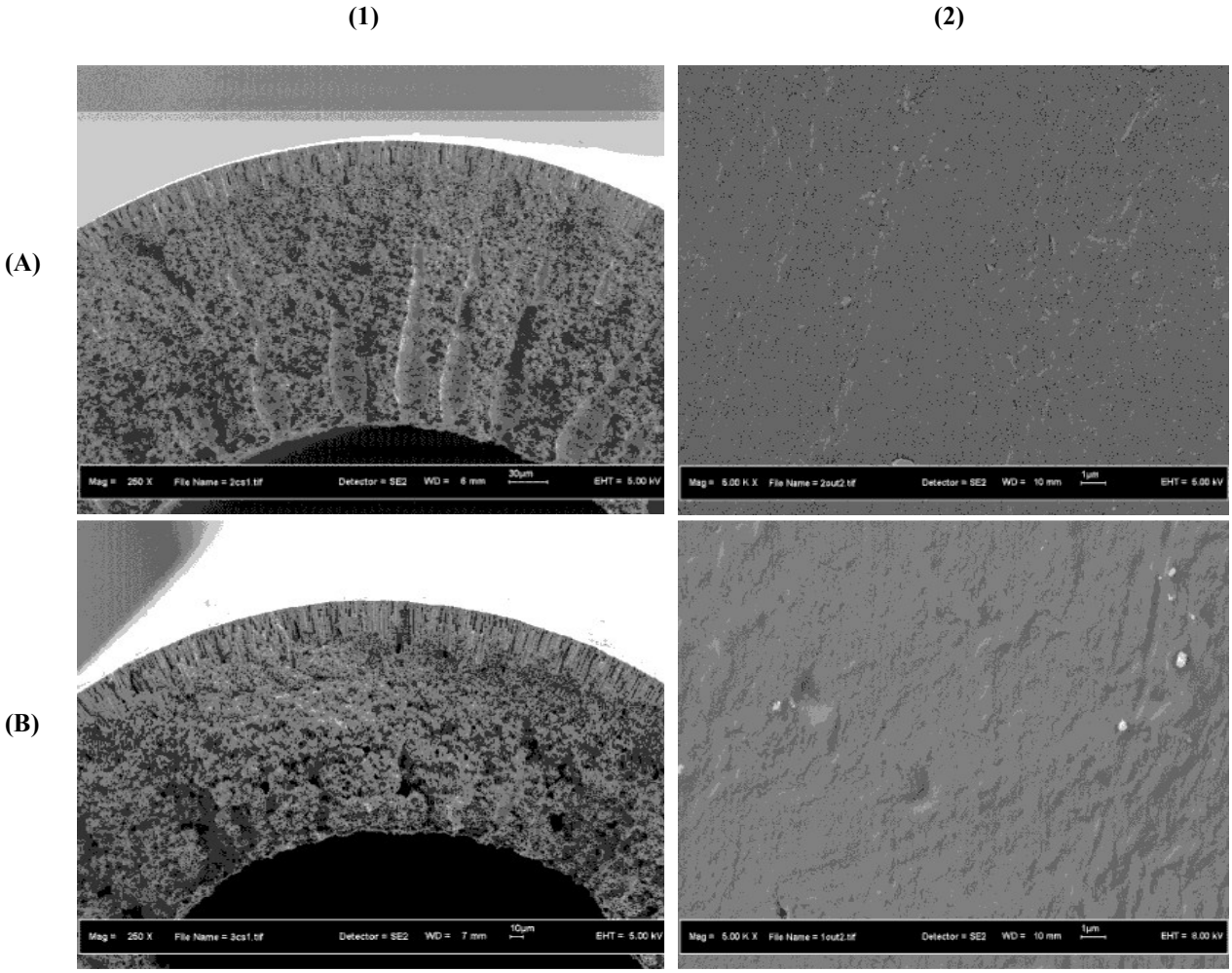

Fig. 1: SEM morphological images of the PVDF hollow fiber membranes: (A) plain PVDF (M0); (B) 5%MMT-filled PVDF (M5); (1) cross-section; (2) outer surface.

The coagulant (water), on the other hand, penetrates into the spinning dope of PEI which is more hydrophilic than PVDF. Hence, the PEI membranes were unsurprisingly formed in the faster phase inversion than PVDF and in turn, a fully finger-like arrangement sandwiched between the inner and outer skin layers could be constructed (see Fig. 2). The addition of hydrophobic MMT clay particles into the hydrophilic PEI affected both the thermodynamic and kinetic aspects of the phase inversion process in a similar manner as it did on the PVDF solutions. MMT embedment lowered thermodynamic stability of PEI solutions [4, 32]. A thin skin layer as a result

could be formed instantaneously when the polymer solution of less thermodynamic stability came into contact with the coagulant (water). As for the kinetic effect of the added MMT filler, there were two opposing effects. A decrease in the solution viscosity as stated earlier was the first effect (see Table 3), as similar to the PVDF dopes. The other effect that was in contrary to the PVDF solutions was due to the higher hydrophobicity of the modified MMT particles than the hydrophilic PEI base polymer, which slowed down the water influx into the nascent membranes was, resulting in the construction of a thicker skin layer and smaller pore size than the pristine PEI membrane. Subsequently, the formed skin layer at the coagulant (water)/polymer solution interface acted as a barrier, contributing to further slowing down of the solvent/coagulant exchange rate. As well, the high hydrophobicity of the added MMT clay particles reduced the mutual affinity of solvent with nonsolvent. Hence, the phase separation changed from instantaneous to delayed demixing. As consequences, more compact sublayer structure and narrower finger-like macrovoids were formed in the PEI MMMs (see Fig. 2) in comparison with the pristine PEI membrane were created.

The interpretation could be supported where practically no interconnectivity between macrovoids in the middle section of the PEI MMMs' cross-sectional micrograph is observed (see Fig. 2 (B1)). It might be ascribed to the lower rate of solvent outflow in a delayed phase inversion, which did not allow some solvent to leave the middle section of the nascent MMMs and the macrovoids were mutually isolated. In other words, the formation of walls between macrovoids was restricted during the decelerated phase inversion and solidification process. Consequently, a combination of many small wall-less macrovoid pores created an empty space in the intermediate layer of the PEI MMMs. The obtained new configuration for PEI MMMs will be

under further confirmation in the later sections by conducting gas permeation test and wetting resistance measurement.

It was therefore concluded that the kinetic effect of the filler contents on the morphology is more important than the thermodynamic effect, when the host polymer is PEI via governing the solvent/-coagulant exchange rate. As well, the effect of MMT clay loading on the membrane morphology is more pronounced for the PEI than PVDF, since the difference in hydrophobicity between PEI and modified MMT clay is more than the difference between PVDF and modified MMT clay.

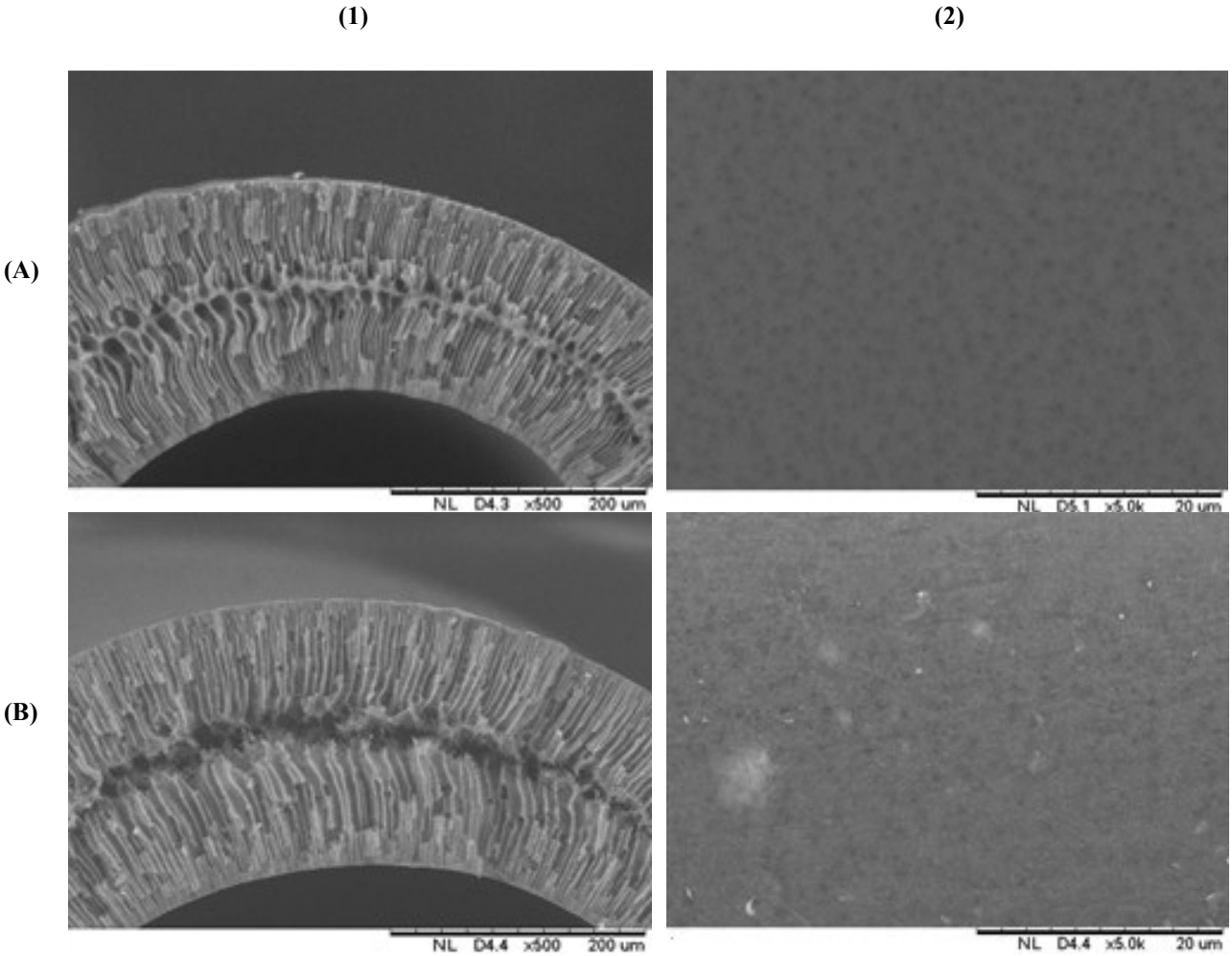

Fig. 2: SEM morphological images of the PEI hollow fiber membranes: (A) plain PEI (P0); (B) 1% MMT-filled PEI (P1); (1) cross section; (2); outer surface.

The results of gas permeation test are illustrated in Fig. 3 where the solid lines are used to measure the pore size and the effective porosity that are shown in Table 3. The results are in good agreement with the morphology of the membranes observed by SEM.

From Table 3, the pore size of the PVDF MMMs did not change very much while the effective porosity increased considerably with an increase in the filler loading from M0 to M3 and then slightly decreased from M3 to M5. The increase in the effective porosity from M0 to M3 is in

accordance with the thinning of the skin layer at the surfaces and the sponge-like layer in the central region of the hollow fiber, which was caused by the thermodynamic instability and the solvent/nonsolvent exchange rate, both increased by the filler incorporation in PVDF. The decrease of the pore size and effective porosity from M3 to M5 is likely ascribed to the enhancement particle aggregation that led to the partial pore blocking. Looking into Fig. 3 (A), the permeation fluxes are exactly in the same order as found in the pore size and the effectively porosity (Table 3), i.e. M0<M1<M3>M5.

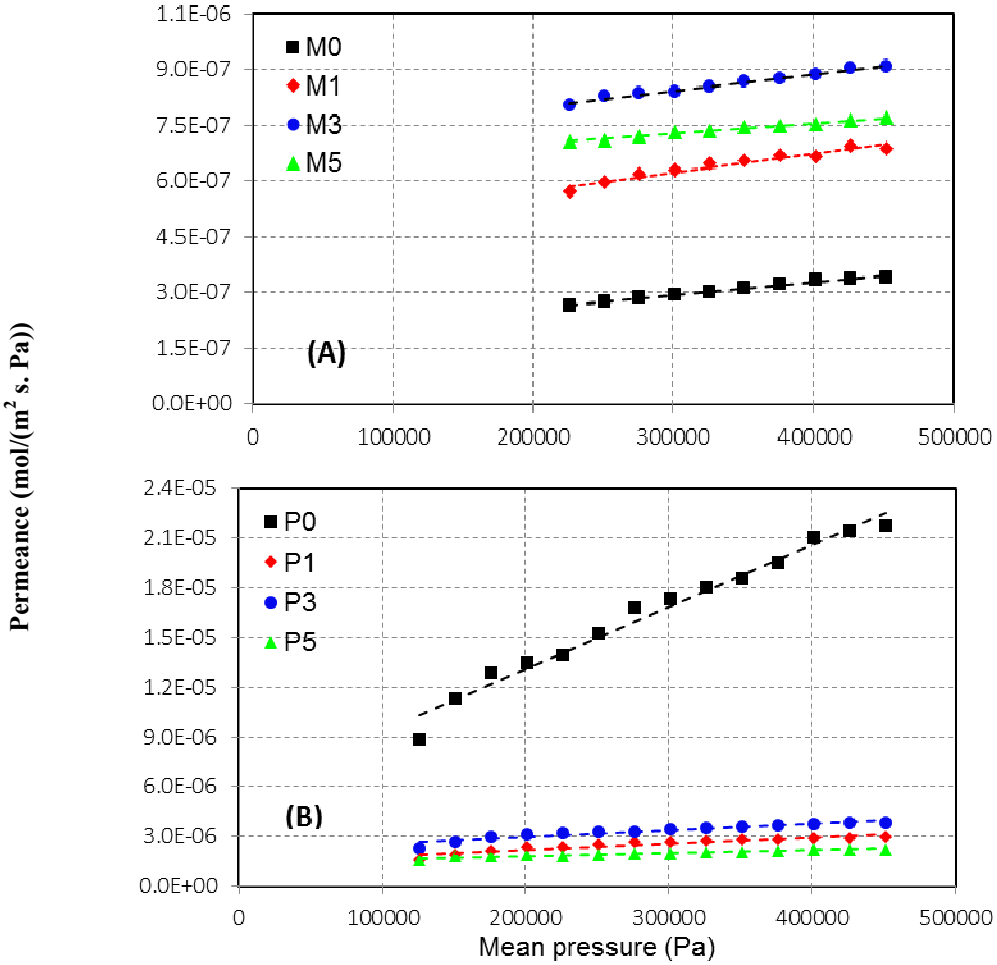

Fig. 3: Measured N_2 permeance of the prepared hollow fiber MMMs as a function of mean pressure; (A): PVDF; (B): PEI.

In contrast to PVDF, the gas permeance of PEI MMMs decreased considerably from the pristine PEI hollow fiber with the order P0 >> P3> P1>P5. This order is close to that found in the pore size (Table 3) P0 >> P1 >P3 > P5, while the change in the effective porosity is in almost reverse order of P0 < P1<P3 >P5. Hence it can be concluded that the change in the gas permeance is due to thickening of the skin layer and the reduction in the size of the finger-like voids, which was caused by the slower solvent/nonsolvent exchange rate at the higher filler loading.

It is interesting to note that the incorporation of modified MMT nanoparticles has an opposite effect on the gas permeance of PVDF and PEI membranes, in the former the filler incorporation increases the gas permeance while in the latter permeance is decreased.

Mechanical stability of membranes is of major importance, as it is required to prevent breakage and deformation of the hollow fiber at high pressures. The mechanical stability of the fabricated membranes was evaluated in terms of collapsing pressure. The results revealed that PVDF membranes have higher mechanical stability than PEI counterparts (Table 3). It was related to the almost the sponge-like structure of the PVDF hollow fibers in comparison with the fully finger-like morphology of the PEI hollow fibers. Moreover, the viscosities of PVDF solutions are higher than PEI solutions, which render a more compact structure than PEI, resulted in higher collapsing pressure. It was reported that the membranes with sponge-like structure have higher mechanical stability than membranes with finger-like morphology [11].

As well, the collapsing pressure was increased by incorporation of nanofillers in both PVDF and PEI hollow fibers (see Table 3). It was proved by other researchers that the addition of a small

amount of the clay fillers into the soft polymeric materials could significantly enhance the mechanical stability of MMMs [33, 34].

Table 3: Characteristics of the prepared hollow fiber membranes.

	M0	M1	M3	M5	P0	P1	P3	P5
Solution viscosity (centipoise)	1250	740	665	590	506	169	279	200
Permeance of N_2 gas at 7 barg	3.70E-07	6.60E-07	8.75E-07	7.72E-07	2.17E-05	2.95E-06	3.86E-06	2.16E-6
Effective surface porosity (ζ / L_P) (m^{-1})	48	74	348	254	128	170	381	276
Mean pore size, $r_{p,m}$ (nm)	26	31	34	21	331	79	59	44
Contact angle (°)	80 ± 1.3	84 ± 1.5	88 ± 2.5	99 ± 1.5	77 ± 0.5	86 ± 3.0	80 ± 1.5	81 ± 2
Liquid entry pressure of water (bar)	8.5 ± 0.5	10 ± 0.2	10 ± 0.5	11 ± 0.3	1.5 ± 0.5	5.5 ± 0.5	4 ± 0.3	3.5 ± 0.2
Collapsing pressure (bar)	8 ± 0.5	9 ± 0.5	10 ± 0.3	11 ± 0.6	2 ± 0.1	4 ± 0.5	4.5 ± 0.2	5 ± 0.3

The average static contact angle of the membranes is also reported in Table 3. Where the PVDF membranes exhibit considerably higher surface contact angles than PEI, which is expected since PVDF is more hydrophobic than PEI. Moreover, the incorporation of hydrophobic MMT particles considerably enhanced the surface contact angle of both PVDF and PEI

Liquid entry pressure of water (LEPw) test was performed to determine the minimum pressure needed to water pass through the biggest pores of the membranes. To minimize the penetration of the liquid absorbent into the membrane pores in contactor application, the operating pressure should not exceed LEPw [10]. The test results were presented in Table 3 where the PVDF

membrane possessed significantly higher LEPw than PEI. It was most likely ascribed to the higher surface hydrophobicity as well as the smaller pore size of PVDF membrane in comparison with those of PEI. Considerable improvement in the LEPw of both PVDF and PEI membranes was observed with the presence of hydrophobic clay particles that was ascribed to increasing surface contact angle as well as reducing pore size of the membrane surface by the addition of MMT.

In particular, the maximum contact angle and LEPw values were achieved for PVDF MMMs at the highest MMT loading of 5 wt.% (M5) while for the PEI MMMs, those were the maximum at MMT loading of 1 wt.% (P1). It indicates that the dispersion of high hydrophobicity clay filler into hydrophobic PVDF solutions is much higher than the hydrophilic PEI. It could be confirmed where the agglomerated parts were observed on the surface of PEI MMMs in SEM images (see Fig. 2 (B2)), while the surface of PVDF MMM was smooth (Fig. 1 (B2)). As the nanoparticles aggregate, the nanoparticle-polymer interfacial area will become smaller, decreasing the high hydrophobicity effect of the MMT on the contact angle and LEPw at high clay loadings.

The fabricated PVDF MMMs having high surface contact angle and LEPw may render higher CO_2 absorption performance stability during long-term operations.

3.2. CO_2 absorption performance of the membranes: Short-term and long-term

Physical CO_2 absorption with distilled water and pure CO_2 as absorbent and solute gas respectively in a short period of time was conducted. The absorption flux was plotted versus

liquid velocity in Fig. 4 with respect to PVDF (A) and PEI (B) hollow fibers with and without filler loading.

For all hollow fibers the flux tends to increase with the increase in the liquid velocity and then levels off, due to the increase in mass transfer coefficient at the liquid boundary layer [35]. However, increasing liquid velocity seems to have a threshold, since the liquid velocity exceeding a specific value (V_c) considerably decreases the gas/liquid contact time and the time of dissolved CO_2 to shift from gas side to the liquid. As a result, the absorption flux above V_c levels off as reported elsewhere [20, 36, 37]. This critical liquid velocity depends on the membrane mass transfer resistance. A membrane sublayer with finger-like structure and a surface with high surface contact angle, porosity and pore size can render high short-term performance and V_c.

The nano-particle loaded MMMs showed significantly higher absorption flux than the pristine membranes where the M5 and P1 possessed the maximum absorption fluxes (see Fig. 4). It can be observed that the CO_2 flux of M5 with the highest absorption flux among PVDF MMMs continues to increase even at the high liquid velocities whereas the flux of M0 starts to level off earlier. Similarly, the flux of P1 keeps increasing while that of P0 levels off. In other words, the membrane of lower flux starts to level off earlier at lower liquid velocity. This is because the membrane starts to control the overall resistance earlier when the intrinsic mass transfer resistance of the membrane is high.

Overall, the effect of the incorporation of the modified MMT on the CO_2 flux is more pronounced for PEI hollow fiber, i.e. by increasing liquid velocity from 0.34 to 2.5 m s^{-1}, the

CO_2 flux of P1 (PEI hollow fiber of the highest flux) increased from 8×10^{-4} mol m^{-2} s^{-1} to 2.2×10^{-3} mol m^{-2} s^{-1} corresponding to 175% improvement; meanwhile the M5 (PVDF hollow fiber of the highest flux) demonstrated 127% enhancement in the flux when the liquid velocity was increased from 0.34 to 2.5 m s^{-1}. This is due to the fully developed finger-like structure of PEI hollow fibers, which allowed to decrease the intrinsic membrane mass transfer resistance.

It is interesting to note that the order in the CO_2 flux of PVDF hollow fiber is M5 > M3 > M1 > M0, which is close to the order in the N_2 gas permeance M3 > M5 > M1 > M0. Undoubtedly, the pristine PVDF hollow fiber exhibited the lowest flux for both CO_2 flux and N_2 permeance. In the case of PEI hollow fiber, the order in the CO_2 gas flux is P1 > P3 > P5 > P0, which is almost the reverse order of N_2 gas permeance P0 > P3 > P1 > P5. In other words, the pristine PEI hollow fiber showed the lowest CO_2 flux whereas it showed the highest N_2 gas permeance. This can be explained by the highest hydrophilicity (contact angle of 77^o), the largest pore size (331 nm) and the lowest LEPw (1.5 bar) of the pristine PEI hollow fiber, which allowed the partial wetting of the pores, resulting in the largest mass transfer resistance of the membrane and the lowest CO_2 flux among all the hollow fibers.

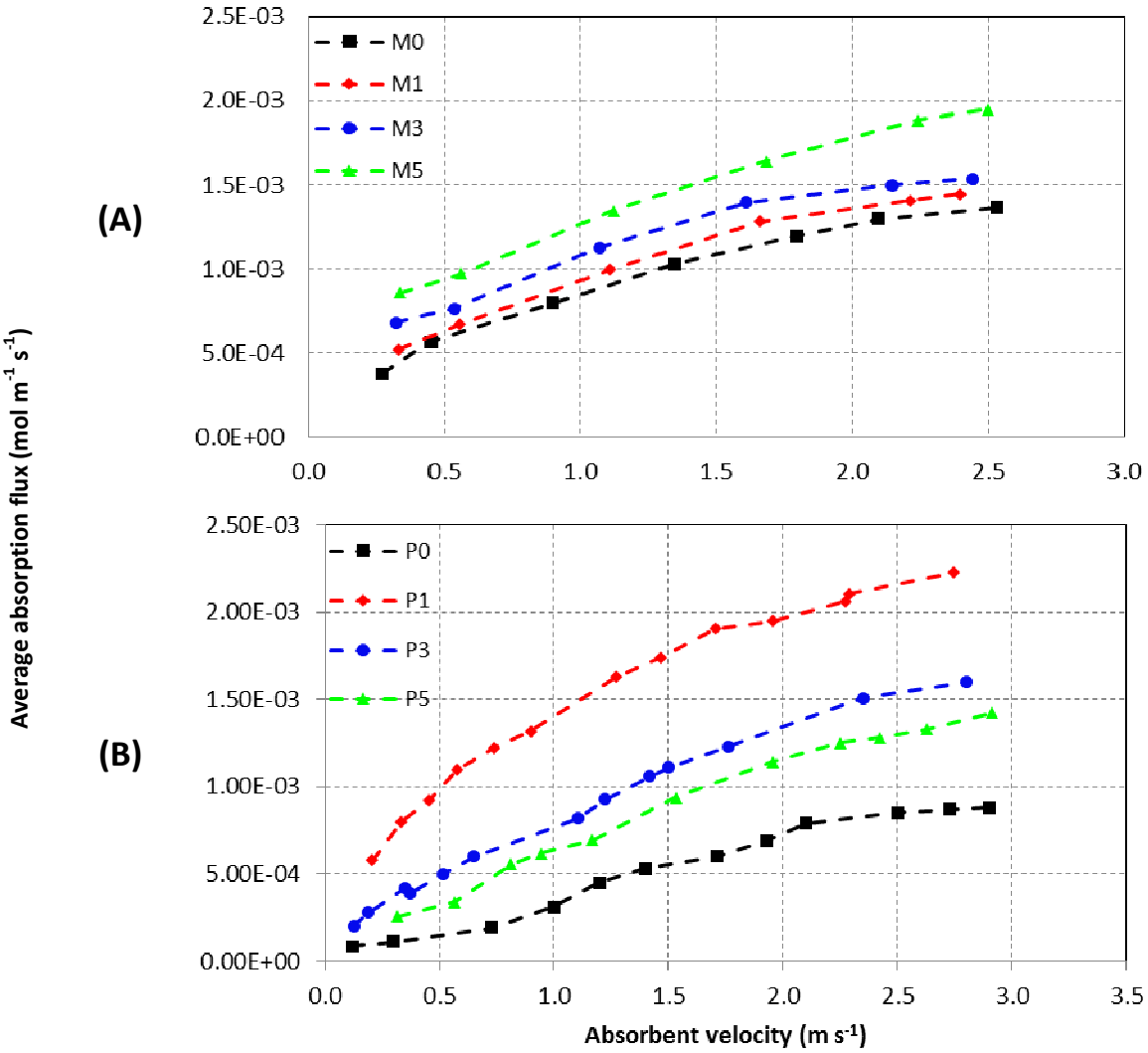

Fig. 4: Variation of average absorption flux of fabricated membranes with liquid velocity A) PVDF membranes B) PEI membranes; distilled water in lumen side; pure CO_2 in shell side (Q_g = 1.2 l/min, T=26 °C, $P_g = 1 \times 10^5$ Pa, $P_l = 1.5 \times 10^5$ Pa).

Although a comparison between short-term contactor test results of the fabricated membranes with embedded clay particles renders the first choice, however, in order to implement an industrial aspect, it is necessary to perform a long-term contactor performance study. Therefore, membranes M5 and P1, which exhibited the highest CO_2 absorption fluxes among fabricated membranes in the short-term contactor test, were subjected to the long-term absorption test. The

results are illustrated in Fig. 5 where M5 MMM almost followed a non-wetted operation mode over 350 hrs (15 days). However, the absorption flux of P1 MMM continuously deteriorated over 250 hrs operation and the test could not be continued due to observation of water droplets in the gas side. The measured flux value after 250 hours for P1 was approximately 106% lower than the initial absorption flux. The performance deterioration was attributed to the increase of the wetted pore volume that did not occur for PVDF MMM.

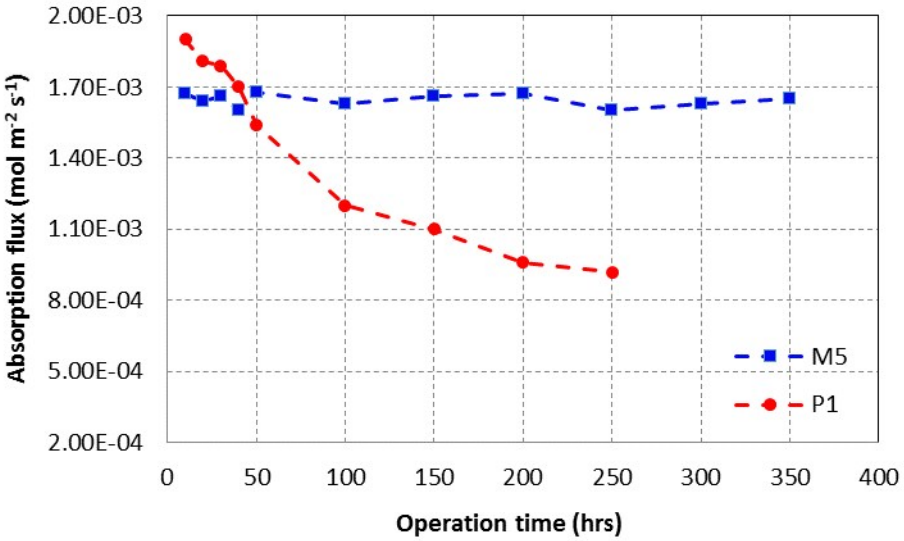

Fig. 5: Long-term stability of PVDF and PEI MMMs (gas: pure CO_2, liquid: pure water, Q_L = 150 mL/m, Q_g = 1.2 L/min, T = 26°C, P_g = 1 bar, P_l = 1.5 bar).

The above results indicate that the hydrophobic polymers are more desirable to maintain long term stability for the gas-liquid contactor process. Furthermore, they make possible to predict the hydrophobic inorganic particles-induced changes in the morphology and in the pore size, porosity and permeance of the PVDF membranes, which affect the gas/liquid contactor performance.

4. Conclusion

Porous PVDF and PEI hollow fiber membranes with different loadings of hydrophobic MMT were fabricated via wet phase inversion method for CO_2 absorption via membrane contactor. The effect of hydrophobic MMT incorporation on the properties of the hollow fiber was significantly different depending on whether the host polymer is either hydrophobic or hydrophilic. When the MMT was embedded in hydrophobic PVDF, the skin layer became thinner, the finger like pores became longer while the sponge-like layer became thinner, resulting in higher N_2 gas permeance. On the contrary, the skin layer became thicker and the finger-like pores became narrower when the MMT was embedded into hydrophilic PEI, resulting is considerably lower N_2 gas permeance. Despite the high N_2 permeance of the pristine PEI hollow fibers, CO_2 absorption flux was unexpectedly low due to the wetting of their large pores. As well, the long term stability of the MMT incorporated PEI hollow fiber was significantly lower compared to the PVDF counterpart, because of the intrinsically hydrophilic nature of PEI, which caused the gradual pore wetting.

Acknowledgement

The authors would like to gratefully and sincerely thank for the research grant funded by Universiti Teknologi Malaysia (UTM) under Pos Doc RU Grant (Vot No. Q. J130000. 21A2. 02E26).

Nomenclature

A	contact area (m^2)
C_L	solute gas concentration in liquid (mol m^{-3})
C_g	solute gas concentration in gas (mol m^{-3})
ΔC_l^{av}	logarithmic mean of the difference in the concentration of solute gas in liquid phase ($mol\ m^{-3}$)

dp	pore diameter (m)
di	inner diameter of hollow fiber (m)
do	outer diameter of hollow fiber (m)
d_{lm}	log mean diameter (m)
H	Henry's constant
Jav	average absorption flux (mol m^2 s^{-1})
K_{OL}	overall mass transfer coefficient (m s^{-1})
k_L	liquid side mass transfer coefficient (m s^{-1})
k_g	gas side mass transfer coefficient (m s^{-1})
k_m	membrane mass transfer coefficient (m s^{-1})
L	hollow fiber membrane length (m)
L_p	effective pore length (m)
M	molecular weight (g mol^{-1})
H	Henry's law constant
p	pressure (pa)
$\bar{p}$	mean pressure (Pa)
$\bar{P}$	total gas permeance (mol m^{-2})
P_p	gas permeance by Poiseuille flow regime (mol $m^{-2}Pa^{-1}$ s^{-1})
P_K	gas permeance by Knudsen flow regime (mol $m^{-2}Pa^{-1}$ s^{-1})
Q_L	liquid flow rate (m^{-1})
r_p	pore radius (m)
$r_{p,m}$	mean pore radius (m)
R	universal gas constant (8.314 J mol^{-1} K^{-1})
T	temperature (K)
V_l	liquid velocity in lumen side (m s^{-1})
ζ	surface porosity
θ	surface contact angle
μ	gas viscosity (Pa s)

References

1. N. Boucif, J. P. Corriou, D. Roizard and E. Favre, AIChE Journal, 2012, 58, 2843-2855.
2. A. Mansourizadeh and A. F. Ismail, Journal of Membrane Science, 2010, 348, 260-267.
3. S. Atchariyawut, C. Feng, R. Wang, R. Jiraratananon and D. Liang, Journal of Membrane Science, 2006, 285, 272-281.
4. E. Fontananova, J. C. Jansen, A. Cristiano, E. Curcio and E. Drioli, Desalination, 2006, 192, 190-197.
5. J. Kong and K. Li, Journal of Applied Polymer Science, 2001, 81, 1643-1653.
6. R. Naim, A. F. Ismail and A. Mansourizadeh, Journal of Membrane Science, 2012, 392–393, 29-37.

7. S. Rajabzadeh, S. Yoshimoto, M. Teramoto, M. Al-Marzouqi and H. Matsuyama, Separation and Purification Technology, 2009, 69, 210-220.
8. A. F. Ismail and A. Mansourizadeh, Journal of Membrane Science, 2010, 365, 319-328.
9. S. Bonyadi, T. S. Chung and R. Rajagopalan, AIChE Journal, 2009, 55, 828-833.
10. G. Bakeri, A. F. Ismail, M. R. DashtArzhandi and T. Matsuura, Journal of Membrane Science, 2015, 475, 57-64.
11. A. Mansourizadeh and A. F. Ismail, International Journal of Greenhouse Gas Control, 2011, 5, 374-380.
12. A. Mansourizadeh, Z. Aslmahdavi, A. F. Ismail and T. Matsuura, International Journal of Greenhouse Gas Control, 2014, 26, 83-92.
13. G. Bakeri, A. F. Ismail, D. Rana and T. Matsuura, Chemical Engineering Journal, 2012, 198–199, 327-337.
14. S. Sinha Ray and M. Okamoto, Progress in Polymer Science, 2003, 28, 1539-1641.
15. P. Wang, J. Ma, Z. Wang, F. Shi and Q. Liu, Langmuir, 2012, 28, 4776-4786.
16. K. Yano, A. Usuki, A. Okada, T. Kurauchi and O. Kamigaito, Journal of Polymer Science Part A: Polymer Chemistry, 1993, 31, 2493-2498.
17. M. Tomaszewska, Desalination, 1996, 104, 1-11.
18. A. Bottino, G. Capannelli, S. Munari and A. Turturro, Desalination, 1988, 68, 167-177.
19. A. F. Ismail, I. R. Dunkin, S. L. Gallivan and S. J. Shilton, Polymer, 1999, 40, 6499-6506.
20. G. Bakeri, T. Matsuura and A. F. Ismail, Journal of Membrane Science, 2011, 383, 159-169.
21. G. Bakeri, A. F. Ismail, M. Shariaty-Niassar and T. Matsuura, Journal of Membrane Science, 2010, 363, 103-111.
22. S. Lee, G. Park, G. Amy, S.-K. Hong, S.-H. Moon, D.-H. Lee and J. Cho, Journal of Membrane Science, 2002, 201, 191-201.
23. H. Yasuda and J. T. Tsai, Journal of Applied Polymer Science, 1974, 18, 805-819.
24. G. Bakeri, A. F. Ismail, D. Rana, T. Matsuura and M. Shariaty, Journal of Applied Polymer Science, 2012, 123, 2812-2827.
25. P. Luis, B. Van der Bruggen and T. Van Gerven, Journal of Chemical Technology & Biotechnology, 2011, 86, 769-775.
26. J. H. Kim, B. R. Min, J. Won, H. C. Park and Y. S. Kang, Journal of Membrane Science, 2001, 187, 47-55.
27. H. J. Kim, R. K. Tyagi, A. E. Fouda and K. Ionasson, Journal of Applied Polymer Science, 1996, 62, 621-629.
28. P. Aerts, I. Genne, S. Kuypers, R. Leysen, I. F. J. Vankelecom and P. A. Jacobs, Journal of Membrane Science, 2000, 178, 1-11.
29. D. Huang, B. Mu and A. Wang, Materials Letters, 2012, 86, 69-72.
30. X. Zhang, W.-Z. Lang, H.-P. Xu, X. Yan and Y.-J. Guo, RSC Advances, 2015, 5, 21532-21543.
31. W. Li, X. Sun, C. Wen, H. Lu and Z. Wang, Front. Environ. Sci. Eng., 2013, 7, 492-502.
32. D. B. Mosqueda-Jimenez, R. M. Narbaitz, T. Matsuura, G. Chowdhury, G. Pleizier and J. P. Santerre, Journal of Membrane Science, 2004, 231, 209-224.
33. K. Y. Wang, S. W. Foo and T.-S. Chung, Industrial & Engineering Chemistry Research, 2009, 48, 4474-4483.

34. J.-M. Yeh, C.-L. Chen, Y.-C. Chen, C.-Y. Ma, H.-Y. Huang and Y.-H. Yu, Journal of Applied Polymer Science, 2004, 92, 631-637.
35. M. Rezaei Dasht Arzhandi, A. F. Ismail and T. Matsuura, RSC Advances, 2015, DOI: 10.1039/C5RA00998G.
36. M. Rezaei DashtArzhandi, A. F. Ismail, T. Matsuura, B. C. Ng and M. S. Abdullah, Chemical Engineering Journal, 2015, 269, 51-59.
37. S. Atchariyawut, C. Feng, R. Wang, R. Jiraratananon and D. T. Liang, Journal of Membrane Science, 2006, 285, 272-281.